

# The Matsu Wheel: A Cloud-based Framework for the Efficient Analysis and Reanalysis of Earth Satellite Imagery

Maria T. Patterson\*, Nikolas Anderson\*, Collin Bennett<sup>†</sup>, Jacob Bruggemann\*, Robert L. Grossman\*<sup>†</sup>, Matthew Handy<sup>‡</sup>, Vuong Ly<sup>‡</sup>, Daniel J. Mandl<sup>‡</sup>, Shane Pederson<sup>†</sup>, James Pivarski<sup>†</sup>, Ray Powell\*, Jonathan Spring\*, Walt Wells<sup>§</sup>, and John Xia\*

\*Center for Data Intensive Science  
University of Chicago, Chicago, IL 60637  
mtpatter@uchicago.edu

<sup>†</sup>Open Data Group  
River Forest, IL 60305

<sup>‡</sup>NASA Goddard Space Flight Center  
Greenbelt, MD 20771

<sup>§</sup>Open Commons Consortium

**Abstract**—Project Matsu is a collaboration between the Open Commons Consortium and NASA focused on developing open source technology for the cloud-based processing of Earth satellite imagery. A particular focus is the development of applications for detecting fires and floods to help support natural disaster detection and relief. Project Matsu has developed an open source cloud-based infrastructure to process, analyze, and reanalyze large collections of hyperspectral satellite image data using Open-Stack, Hadoop, MapReduce, Storm and related technologies.

We describe a framework for efficient analysis of large amounts of data called the Matsu “Wheel.” The Matsu Wheel is currently used to process incoming hyperspectral satellite data produced daily by NASA’s Earth Observing-1 (EO-1) satellite. The framework is designed to be able to support scanning queries using cloud computing applications, such as Hadoop and Accumulo. A scanning query processes all, or most of the data, in a database or data repository.

We also describe our preliminary Wheel analytics, including an anomaly detector for rare spectral signatures or thermal anomalies in hyperspectral data and a land cover classifier that can be used for water and flood detection. Each of these analytics can generate visual reports accessible via the web for the public and interested decision makers. The resultant products of the analytics are also made accessible through an Open Geospatial Compliant (OGC)-compliant Web Map Service (WMS) for further distribution. The Matsu Wheel allows many shared data services to be performed together to efficiently use resources for processing hyperspectral satellite image data and other, e.g., large environmental datasets that may be analyzed for many purposes.

## I. INTRODUCTION

The increasing availability of large volumes of scientific data due to the decreasing cost of storage and processing power has led to new challenges in scientific research. Scientists are finding that the bottleneck to discovery is no longer a lack of data but an inability to manage and analyze their large datasets.

A common class of problems require applying an analytic computation over an entire dataset. Sometimes these are called *scanning queries* since they involve a scan of the entire dataset. For example, analyzing each image in a large collection of images is an example of a scanning query. In contrast, standard queries typically process a relatively small percentage of the data in a database or data repository.

With multiple scanning queries that are run within a time that is comparable to the length of time required for a single scan, it can be much more efficient to scan the entire dataset once and apply each analytic in turn versus scanning the entire dataset for each scanning query as the query arrives. This is the case unless the data management infrastructure has specific technology for recognizing and processing scanning queries. In this paper, we introduce a software application called the Matsu Wheel that is designed to support multiple scanning queries over satellite imagery data.

Project Matsu is a collaborative effort between the Open Science Data Cloud (OSDC), managed by the Open Commons Consortium (OCC), and NASA, working to develop open source tools for processing and analyzing Earth satellite imagery in the cloud. The Project Matsu “Wheel” is a framework for simplifying Earth satellite image analysis on large volumes of data by providing an efficient system that performs all the common data services and then passes the prepared chunks of data in a common format to the analytics, which processes each new chunk of data in turn.

### A. Motivation for an analytic wheel

The idea behind the wheel is to have all of the data processing services performed together on chunks of data to efficiently use resources, including available network bandwidth, access to secondary storage, and available computing resources. This is especially important with reanalysis, in which the entire

dataset is processed using an updated algorithm, a recalibration of the data, a new normalization of the data, a new workflow, etc. The motivation behind the analytic wheel is to streamline and share these services so that they are only performed once on each chunk of data in a scanning query, regardless of the number or type of scanning analytics run over the data.

### B. Comparison to existing frameworks

The Matsu Wheel approach differs from other common data management or data processing systems. Real-time distributed data processing frameworks (for example, Storm, S4, or Akka) are designed to process data in real time as it flows through a distributed system (see also, e.g., [1], [2], [3]). In contrast, the Wheel is designed for the reanalysis of an entire static dataset that is stored in distributed storage system (for example, the Hadoop Distributed File System) or distributed database (for example, HBase or Accumulo).

It is important to note, that any distributed scale-out data processing system based upon virtual machines has certain performance issues due to the shared workload across multiple virtual machines associated with a single physical node. In particular, these types of applications may have significant variability in performance for real scientific workloads [4]. This is true, when multiple scanning queries hit a distributed file system, a NoSQL database, or a wheel based system on top of one these infrastructures. When a NoSQL database is used for multiple scanning queries with a framework like the wheel, the NoSQL database can quickly become overloaded.

### C. Application to Earth satellite data

Analyses of Earth satellite data and hyperspectral imagery data in particular benefit from the Matsu Wheel system as a use case in which the data may be large, have high-volume throughput, and are used for many types of applications. The Project Matsu Wheel currently processes the data produced each day by NASA's Earth Observing- 1 (EO-1) satellite and makes a variety of data products available to the community. In addition to the Atmospheric Corrector, the EO-1 satellite has two primary scientific instruments for land observations, the Advanced Land Imager (ALI) and a hyperspectral imager called Hyperion [5], [6]. EO-1 was launched in November 2000 as part of NASA's New Millennium Program (NMP) initiative for advancing new technologies in space and is currently in an extended mission.

The ALI instrument acquires data in 9 different bands from 0.48–2.35  $\mu\text{m}$  with 30-meter resolution plus a panchromatic band with higher 10-meter spatial resolution. The standard scene size projected on the Earth surface equates to 37 km x 42 km (width x length). Hyperion has similar spatial resolution but higher spectral resolution, observing in 242 band channels from 0.357–2.576  $\mu\text{m}$  with 10-nm bandwidth. Hyperion scenes have a smaller standard footprint width of 7.7 km. The Matsu Wheel runs analytics over Level 1G data in Geographic Tagged Image File Format (GeoTiff) format, which have been radiometrically corrected, resampled for geometric correction, and registered to a geographic map projection. The GeoTiff

data and metadata for all bands in a single Hyperion scene can amount to 1.5–2.5 GB of data for only the Level 1G data. A cloud environment for shared storage and computing capabilities is ideal for scientific analysis of many scenes, which can quickly add to a large amount of data.

## II. WORKFLOW

### A. Cloud environment

Project Matsu uses both an OpenStack-based computing platform and a Hadoop-based computing platform, both of which are managed by the OCC ([www.occ-data.org](http://www.occ-data.org)) in conjunction with the University of Chicago. The OpenStack platform (the Open Science Data Cloud [7]) currently contains 60 nodes, 1208 compute cores, 4832 GB of compute RAM, and 1096 TB of raw storage. The Hadoop [8] platform currently contains 28 nodes, 896 compute cores, 261 TB of storage, and 3584 GB of compute RAM.

### B. Pre-processing of data on the OSDC

The Open Science Data Cloud provides a number of data center services for Project Matsu. The data are received daily from NASA, stored on a distributed, fault-tolerant file system (GlusterFS), and pre-processed prior to the application of the Wheel analytics on Skidmore. The images are converted into SequenceFile format, a file format more suited for MapReduce, and uploaded into HDFS [9]. Metadata and compute summary statistics are extracted for each scene and stored in Accumulo, a distributed NoSQL database [10]. The metadata are used to display the geospatial location of scenes via a mapping service so that users can easily visualize which areas of the Earth are covered in the data processed by the Matsu Wheel.

Here is an overview of the Matsu data flow for processing EO-1 images and producing data and analytic products:

- 1) Performed by NASA/GSFC as part of their daily operations:
  - a) Transmit data from NASA's EO-1 Satellite to NASA ground stations and then to NASA/GSFC.
  - b) Align data and generate Level 0 images.
  - c) Transmit Level 0 data from NASA/GSFC to the OSDC.
- 2) Run by NASA on the OSDC OpenStack cloud for Matsu and other projects:
  - a) Store Level 0 images in the OSDC Public Data Commons for long-term, active storage.
  - b) Within the OSDC, launch Virtual Machines (VMs) specifically built to render Level 1 images from Level 0. Each Level 1 band is saved as a distinct image file (GeoTIFF).
  - c) Store Level 1 band images in the OSDC Public Data Commons for long-term storage.
- 3) Run specifically for Project Matsu on the Hadoop cloud:
  - a) Read Level 1 images, combine bands, and serialize image bands into a single file.
  - b) Store serialized files on HDFS.
  - c) Run Wheel analytics on the serialized Level 1 images

stored in HDFS.

d) Store the results of the analysis in Accumulo for further analysis, generate reports, and load into a Web Map Service.

### C. Analytic ‘wheel’ architecture

The analytic Wheel is so named because multiple analytics are applied to data as it flows underneath. While a bicycle or water wheel does not fit exactly, the image is clear: do the work as the data flows through once, like the pavement under the bicycle wheel. With big data, retrieving or processing data multiple times is an inefficient use of resources and should be avoided.

When new data become available in HDFS as part of the pre-processing described above, the MapReduce scanning analytics kick off. Intermediate output is written to HDFS, and all analytic results are stored in Accumulo as JSON. Secondary analysis that can run from the results of other analytics can be done “off the wheel” by using the Accumulo-stored JSON as input.

As many analytics can be included in the Wheel as can run in the allowed time. If new data are obtained each day, then the limit is 24 hours to avoid back-ups in processing. For other use cases, there may be a different time window in which the results are needed. This can be seconds, minutes, or hours. Our MapReduce analytic environment is not designed to yield immediate results, but the analytics can be run on individual images at a per minute speed. Analytics with results that need to be made available as soon as possible can be configured to run first in the Wheel. We show a diagram of the flow of EO-1 data from acquisition and ingest into HDFS through the analytic Wheel framework in Figure 1.

The Wheel architecture is an efficient framework not restricted only to image processing, but is applicable to any workflow where an assortment of analytics needs to be run on data that require heavy pre-processing or have high-volume throughput.

## III. ANALYTICS

We are currently running five scanning analytics on daily images from NASA’s EO-1 satellite with the Project Matsu Wheel, including several spectral anomaly detection algorithms and a land cover classification analytic. Here we describe each of these and the resulting analytic reports generated.

### A. Contours and Clusters

This analytic looks for contours in geographic space around clusters in spectral space. The input data consist of Level 1G EO-1 GeoTiff images from Hyperion, essentially a set of radiances for all spectral bands for each pixel in an image. The radiance in each band is divided by its underlying solar irradiance to convert to units of reflectivity or at-sensor reflectance. This is done by scaling each band individually by the irradiance and then applying a geometric correction for the solar elevation and Earth-Sun distance, as shown in eqn. 1,

$$\rho_i = \left( \frac{\pi}{\mu_0 F_{0,i} / d_{earth-sun}^2} \right) L_i \quad (1)$$

where  $\rho_i$  is the at-sensor reflectance at channel  $i$ ,  $\mu_0 = \cos(\text{solar zenith angle})$ ,  $F_{0,i}$  is the incident solar flux at channel  $i$ ,  $d_{Earth-Sun}$  is the Earth-Sun distance, and  $L_i$  is the irradiance recorded at channel  $i$  [11]. This correction accounts for differences in the data due to time of day or year.

We then apply a principal component analysis (PCA) to the set of reflectivities, and the top N (we choose N=5) PCA components are extracted for further analysis. There are two passes for the Contours and Clusters analytic to generate a contour result: spectral and spatial.

- Spectral clusters are found in the transformed N-dimensional spectral space for each image using a k-means clustering algorithm and are then ranked from most to least extreme using the Mahalanobis distance of the cluster from the spectral center of the image.
- Pixels are spatially analyzed and are grouped together into contiguous regions with a certain minimum purity or fraction of pixels that belong to that cluster and are then ranked again based on their distance from the spectral cluster center.

Each cluster then has a score indicating 1) how anomalous the spectral signature is in comparison with the rest of the image and 2) how close the pixels within the contour are to the cluster signature. The top ten most anomalous clusters over a given timeframe are singled out for manual review and highlighted in a daily overview summary report.

The analytic returns the clusters as contours of geographic regions of spectral “anomalies” which can then be viewed as polygonal overlays on a map. The Matsu Wheel produces image reports for each image, which contain an interactive map with options for an OpenStreetMap, Google Physical, or Google Satellite base layer and an RGB image created from the hyperspectral data and identified polygon contours as options for overlays. Researchers or anyone interested in the results can view the image reports online through a web browser.

By implementing this analytic in the Matsu Wheel, we have been able to automatically identify regions of interesting activity on the Earth’s surface, including several volcanic events. For example, in February 2014, this Matsu Wheel analytic automatically identified anomalous activity in EO-1 Hyperion data of the Barren Island volcano, which was also confirmed to be active by other sources. We show an example analytic image report for this event in Figure 2.

### B. Rare Pixel Finder

The Rare Pixel Finder (RPF) is an analytic designed to find small clusters of unusual pixels in a hyperspectral image. This algorithm is applied directly to the EO-1 data in radiances, but the data can also be transformed to reflectances or other metrics or can have logs applied.

Using the subset of k hyperspectral bands that are determined to be most informative, it computes k-dimensional

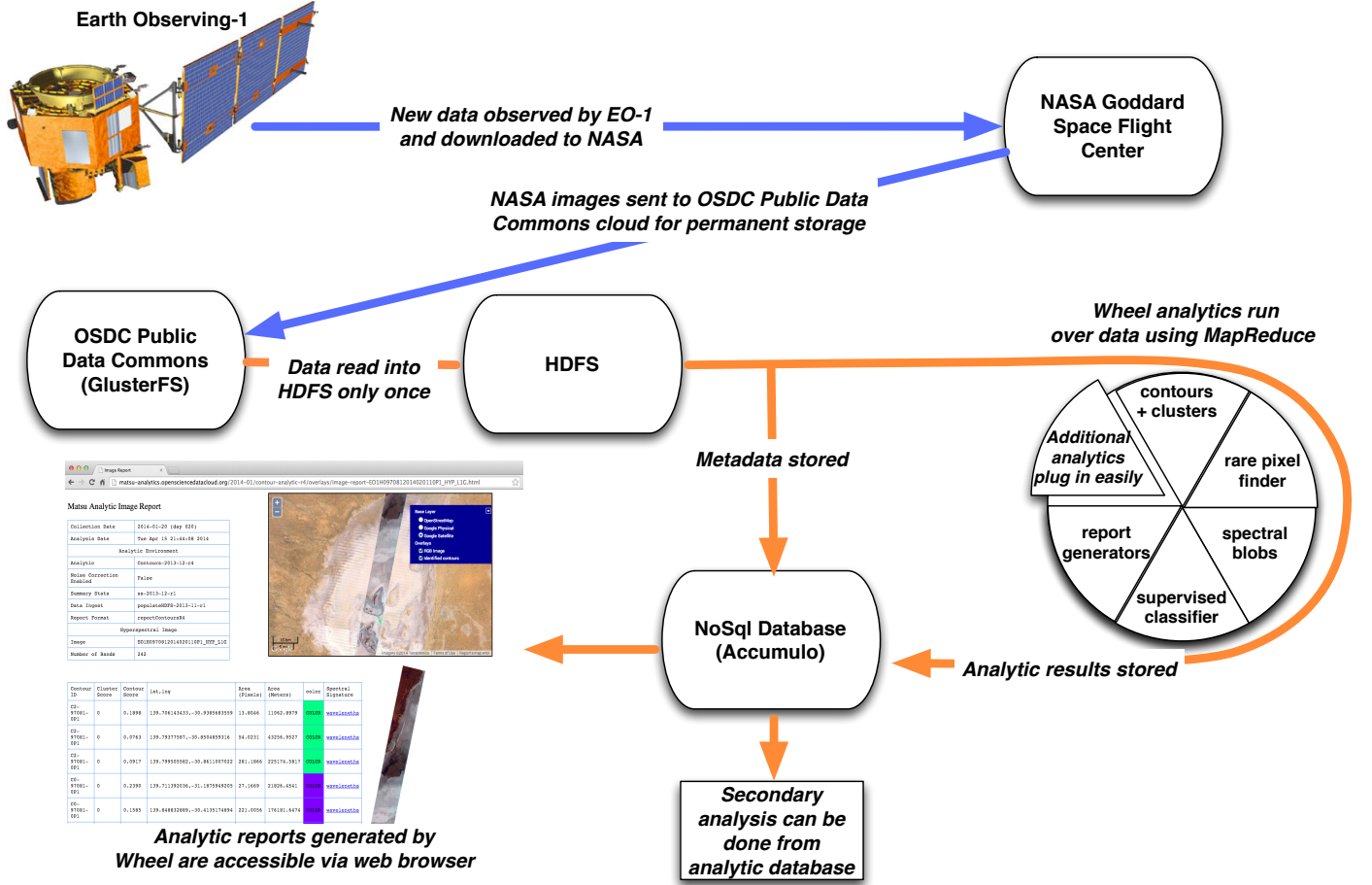


Fig. 1: A diagram of the flow of EO-1 ALI and Hyperion data from data acquisition and ingest through the Wheel framework. Orange denotes the processes performed on the OSDC Skidmore cloud. With the Wheel architecture, the data need to be read in only once regardless of the number of analytics applied to the data. The Matsu Wheel system is unique in that, essentially, the *data* are flowing through the framework while the analytic queries sit in place and scan for new data. Additional analytics plug in easily, with the requirement that an analytic takes as input a batch of data to be processed. An analytic query may be written such that it can be run on its own in the Wheel or written to take as input the output of an upstream analytic. The report generators are an example of the latter case, generating summary information from upstream analytics.

Mahalanobis distances and finds the pixels most distant. From this subset, pixels that are both spectrally similar and geographically proximate are retained. Spectrally similar pixels that can be further grouped into small compact sets are reported as potential outlying clusters. Details of the different steps of the algorithm are given below.

In the pre-processing step, we remove areas of the image that are obvious anomalies not related to the image (e.g., zero radiances on the edges of images), as well as spectral bands that correspond to water absorption or other phenomena that result in near-zero observed radiances. Any transformations are applied to the data at this point, such as transforming radiance to reflectance or logs.

Once the data are pre-processed, the Mahalanobis distance ( $D_i$ ) is calculated for each pixel. Then, only the subset  $S_1$  of pixels that satisfy  $D_i > k_1$  are selected, where  $k_1$  is chosen

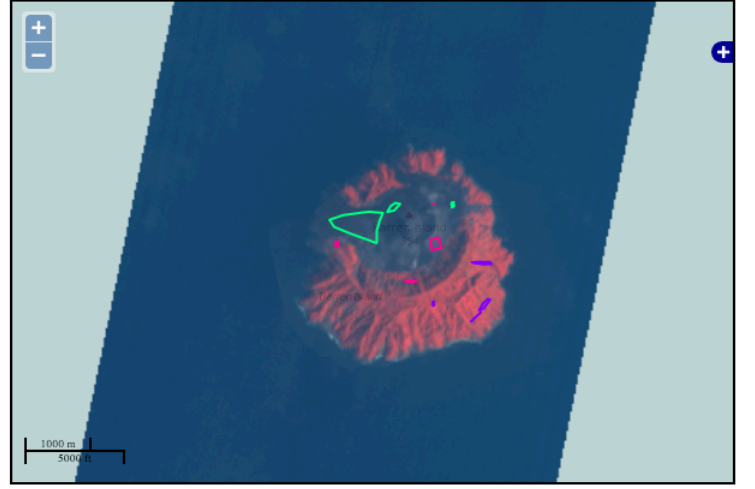
such that  $S_1$  only contains 0.1–0.5% of pixels. In practice  $k_1$  was based on the upper  $6\sigma$  of the distribution of sample distances, assuming a log-normal distribution for the distances.

For the subset of  $S_1$  pixels chosen in the previous step, we next compute a similarity matrix  $T$  with elements  $T_{ij}$  measuring the spectral similarity between each pair of pixels. The similarity metric is based on the dot product between each pair of points and measures the multi-dimensional angle between points. The matrix is only formed for the subset  $S_1$  and contains a few hundred rows. The pixels are then further subsetted. Pixel  $i$  is selected for set  $S_2$  if  $T_{ij} > k_2$  for  $j \neq i$ . The parameter  $k_2$  is chosen to be very close to 1; in this way we select objects that are both spectrally extreme but still have similar spectral profiles to one another.

In order to cluster the pixels geographically, we assume they lie on a rectangular grid. An  $L_1$  norm metric is applied to the

## Matsu Analytic Image Report

Collection Date	2014-02-28 (day 059)
Analysis Date	Fri Feb 28 23:36:46 2014
Analytic Environment	
Analytic	Contours-2013-12-r4
Noise Correction Enabled	False
Summary Stats	ss-2013-12-r1
Data Ingest	populateHDFS-2013-11-r1
Report Format	reportContoursR4
Hyperspectral Image	
Image	EO1H1330512014059110KF_HYP_L1G
Number of Bands	242



Contour ID	Cluster Score	Contour Score	lat,lng	Area (Pixels)	Area (Meters)	color	Spectral Signature
C2-33051-OKF	565	1.5535	93.8578094939,12.2852573399	263.0121	16530.4573	COLOR	<a href="#">wavelengths</a>
C2-33051-OKF	565	1.2823	93.8626806684,12.2876768848	13.7443	863.8411	COLOR	<a href="#">wavelengths</a>
C2-33051-OKF	565	0.6199	93.8711375299,12.2880446336	2.6813	168.5211	COLOR	<a href="#">wavelengths</a>
C0-33051-OKF	961	1.2159	93.8683521272,12.2742196338	1.0556	66.3400	COLOR	<a href="#">wavelengths</a>
C0-33051-OKF	961	1.8826	93.8754336513,12.2798956163	8.9821	564.5147	COLOR	<a href="#">wavelengths</a>

Fig. 2: A screenshot of a Matsu analytic image report for a Contours and Clusters spectral anomaly analytic that automatically identified regions of interest around the Barren Island volcano, confirmed as active by other sources in February 2014. The reports contain basic information about the data analyzed and the analytic products and a zoomable map with the data and analytic products shown as an overlay on an OpenStreetMap, Google Physical, or Google Satellite base layer. In this analytic, interesting regions are given a cluster score from 0 - 1000 based on how anomalous they are compared to the average detection and appear as colored contours over the image.

subset  $S_2$  in order to further whittle down the candidate set to pixels that are spectrally extreme, spectrally similar, and geographically proximate. The metric is set so that traversing from one pixel to an immediately adjacent one would give a distance of 1, as if only vertical and horizontal movements were allowed. Pixel  $i$  is selected for set  $S_3$  if  $M_{ij} < k_3$  for  $j \neq i$  and for some small value of  $k_3$ . We used  $k_3 = 3$ , so that pixels either needed to be touching on a face or diagonally adjacent.

In the final step a simple heuristic designed to find the connected components of an undirected graph is applied. We further restrict to a set  $S_4$  that are geographically proximate to at least  $k_4$  other pixels (including itself). We used  $k_4 = 5$ , with the goal of finding compact clusters of between 5 and 20 pixels in size. The clumping heuristic then returns the pixels that were mapped into a cluster, the corresponding cluster ID's,

and the associated distances for the elements of the cluster.

The flagged pixels are reported as "objects". These groups of objects are further filtered in order to make sure that they actually represent regions of interest. The following criteria must be satisfied in order to qualify:

- 1) *Spectral Extremeness*. The mean Mahalanobis Distance must be greater than or equal to some parameter  $p_1$ . This selects clusters that are sufficiently extreme in spectral space.
- 2) *Spectral Closeness*. The Signal-to-Noise ratio must be greater than or equal to some parameter  $p_2$ . This selects clusters that have similar values of Mahalanobis Distance.
- 3) *Cluster Size*. All clusters must be between a minimum value parameter  $p_3$  and a maximum parameter  $p_4$  pixels in size (the goal of this classifier is to find small

clusters).

- 4) *Cluster Dimension*. All clusters must have at least some parameter  $p_5$  rows and columns (but are not restricted to be rectangles).

Parameters  $p_1 - p_5$  are all tuning parameters that can be set in the algorithm to achieve the desired results.

#### C. Gaussian Mixture Model and K-Nearest Neighbors (GMM-KNN) Algorithm

The Gaussian Mixture Model and K-Nearest Neighbors (GMM-KNN) algorithm is also designed to find small clusters of unusual pixels in a multispectral image. Using 10–30 spectral bands, it fits the most common spectral shapes to a Gaussian Mixture Model (smoothly varying, but makes strong assumptions about tails of the distribution) and also a K-Nearest Neighbor model (more detailed description of tails, but granular), then searches for pixels that are far from common. Once a set of candidate pixels have been found, they are expanded and merged into “clumps” using a flood-fill algorithm. Six characteristics of these clumps are used to further reduce the number of candidates.

In short, the GMM-KNN algorithm consists of the following steps.

- 1) Preprocessing: Take the logarithm of the radiance value of each band and project the result onto a color-only basis to remove variations in intensity, which tend to be transient while variations in color are more indicative of ground objects.
- 2) Gaussian Mixture Model: Fit  $k = 20$  Gaussian components to the spectra of all pixels, sufficiently large to cover the major structures in a typical image.
- 3) Flood-fill: Expand GMM outliers to enclose any surrounding region that is also anomalous, and merge GMM outliers if they are in the same clump.
- 4) Characterizing clumps: Derive a detailed suite of features to quantify each clump, including KNN, edge detection, and the distribution of pixel spectra in the clump.
- 5) Optimizing selection: Choose the most unusual candidates based on their features.

#### D. Spectral Blobs

This algorithm uses a “windowing” technique to create a boundary mask from the standard deviation of neighboring pixels. A catalog of spectrally similar blobs, that contain varying numbers of pixels, is created. This analytic consists of the following steps:

- Label spatially connected components of the mask using an undirected graph search algorithm.
- Apply statistical significance tests (t-test, chi-squared) to the spectral features of the connected component (the “blobs”).
- Merge spectrally similar regions.

The anomalous regions are the small spatial blobs that are not a member of any larger spatial cluster.

#### E. Supervised Spectral Classifier

The Supervised Spectral Classifier is a land coverage classification algorithm for the Matsu Wheel. We are particularly interested in developing these analytics for the detection of water and constructing flood maps to complement the onboard EO-1 flood detection system [12]. This analytic is written to take ALI or Hyperion Level 1G data and classify each pixel in an image as a member of a given class in a provided training set. We currently implement this analytic with a simple land coverage classification training set with four possible classes:

- Clouds
- Water
- Desert / dry land
- Vegetation

The classifier relies on a support vector machine (SVM) algorithm, using the reflectance values of each pixel as the characterizing vector. In this implementation of the classifier, we bin Hyperion data to resemble ALI spectra for ease of use and computation speed in training the classifier. The result of this analytic is a GeoTiff showing the classification at each pixel.

1) *Building a training data set*: We constructed a training data set of classified spectra from sections of EO-1 Hyperion images over areas with known land coverage and cloud coverage and confirmed our selections by visual inspection of three-color (RGB) images created of the training images. We used a combination of Hyperion bands B16 (508.22 nm), B23 (579.45 nm), and B29 (640.5 nm) to construct the RGB images. For each image contributing to the training data set, we only included spectra for collections of pixels that were visually confirmed as exclusively desert, water, clouds, or vegetation.

The training data set consists of approximately 6,000 to 9,000 objects for each class. We include spectra for a variety of different regions on the Earth observed during different times of the year and a range of solar elevation angles. Because absolute values are necessary to directly compare the training data to all test images, the raw irradiance values from the Level 1G data must first be converted to at-sensor reflectance using eqn. 1. Table I lists general properties of the Hyperion scenes used in constructing the training set, where the class column indicates which class(es) (C = cloud, W = water, V = vegetation, and D = desert) that scene contributed to.

We show a plot of the average training set object’s reflectance spectra for each of the four classes (clouds, desert, vegetation, water) in Figure 3, which are in agreement with the expected results. These spectra are consistent with the spectral signatures of cloud, vegetation, and desert sand presented in other examples of EO-1 Hyperion data analysis, specifically Figures 3 and 4 in Griffin, et. al. (2005) [11] [13].

2) *Classifying new data*: The classifier uses the SVM method provided by the Python scikit-learn machine learning package [14]. We construct a vector space from all ALI bands and two additional ALI band ratios, the ratios between ALI bands 3:7 and 4:8. These ratios were chosen because they

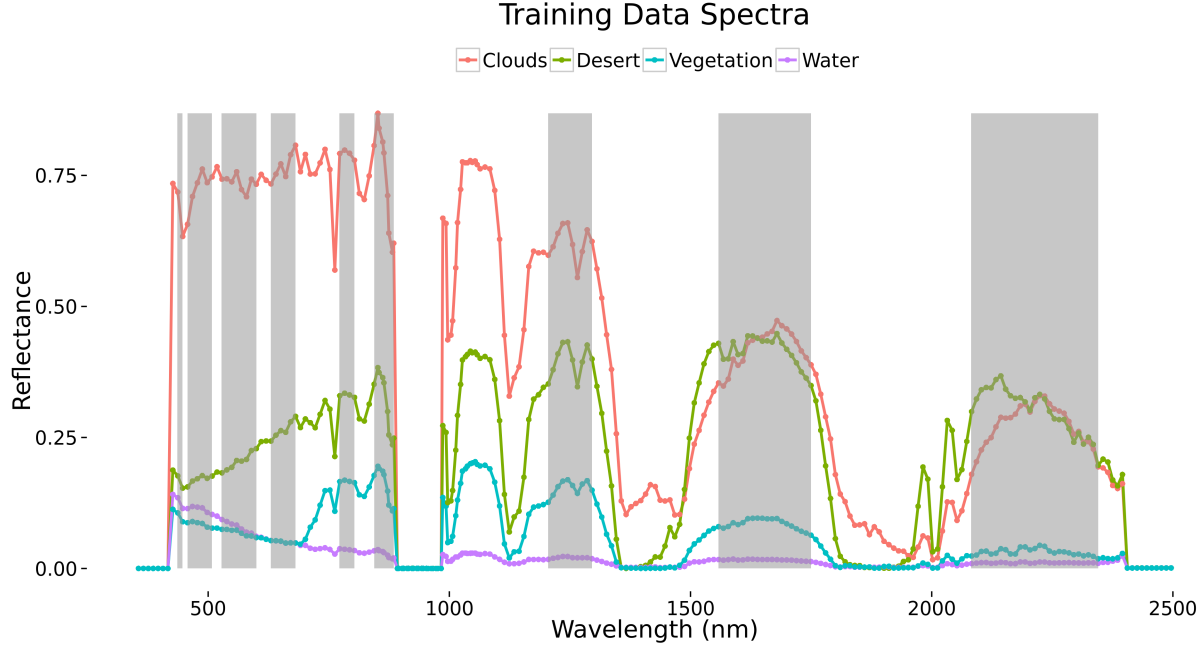


Fig. 3: The average reflectance spectra for each of the four classifications in the training data used by our implementation of the Supervised Spectral Classifier analytic. The four classes are clouds (salmon), desert (lime green), vegetation (cyan), and water (purple). Shaded grey areas show the wavelength coverage of ALI bands, which are the wavelength regions used by the classifier described.

TABLE I: Scenes included in training set

Region name	Class	Obs Date	Sun Azim. (°)	Sun Elev. (°)
Aira	W	4/18/14	119.12	49.1
San Rossore	C/W	1/29/14	145.5	20.9
San Rossore	C/V	8/10/12	135.8	54.5
Barton Bendish	C	8/22/13	142.7	43.5
Jasper Ridge	V/D	9/17/13	140.7	46.9
Jasper Ridge	V/C	9/14/13	132.9	45.2
Jasper Ridge	V/C	9/27/12	147.6	45.4
Arabian Desert	D	12/30/12	147.0	29.9
Jornada	D	12/10/12	28.7	151.4
Jornada	D	7/24/12	59.6	107.5
Negev	D	9/15/12	130.7	52.1
White Sands	C	7/29/12	58.3	108.4
Besetsutzuyu	V	7/14/12	56.8	135.5
Kenatedo	W	6/22/12	50.5	46.5
Santarem	W	6/17/12	57.1	118.15
Bibubemuku	W	5/20/12	57.5	127.7

provided the best individual results in correctly distinguishing between classes when used as the sole dimension for the SVM.

For Hyperion images, bands that correspond to the coverages of the ALI bands are combined. The same corrections to reflectance values that are applied to the training data are applied to the input image data. For ALI data, an additional scale and offset need to be applied before the irradiance values are converted to reflectance.

3) *Validating results:* To confirm that the classifier analytic is generating reasonable results, we compare the fractional amount of land coverage types calculated by the classifier with known fractional amounts from other sources. We compare our

results for classified cloud coverage with the cloud coverage amounts stated for individual scenes available through the EarthExplorer tool from the U.S. Geological Survey (USGS) [15]. We show a visual comparison of cloud coverage determined by our classifier with cloud coverage amounts stated by EarthExplorer for three Hyperion scenes of the big island of Hawaii with varying amounts of clouds and a randomly chosen scene of a section of the coast of Valencia in Figure 4. For each pair of scenes, the left image shows an RGB image of the Hyperion data with the USGS calculated cloud coverage, and the right column has the classified image results, with the amount of cloud coverage classified indicated.

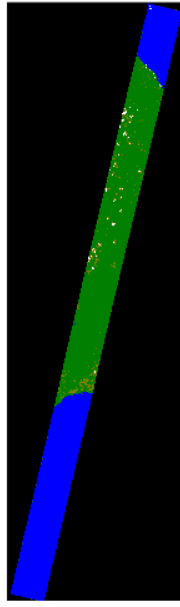
The classified images appear to be visually consistent with RGB images, though the calculations for classified cloud coverage are not in complete agreement with USGS particularly for lower amounts of cloud coverage. This may be because the USGS EarthExplorer images include very thin cloud "haze" in cloud coverage calculations.

In the image of Valencia, Spain, shown in Figures 4g and 4h the classifier can clearly distinguish the coastline in the picture, correctly classifying the water and land features and shows good agreement with regions that appear to be cloud. It has some difficulty in shadowed areas like those regions covered by cloud shadow. In Figure 5, we show a plot comparing expected cloud and water coverage to the coverages determined by our classifier for 20 random test scenes. For each scene, the expected cloud coverage is taken as the center of the range provided by the USGS EarthExplorer summary

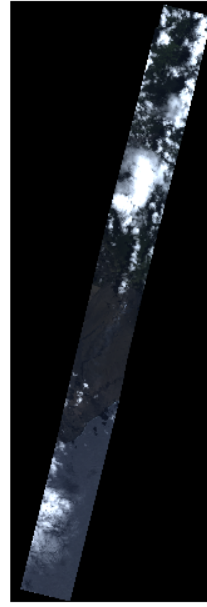




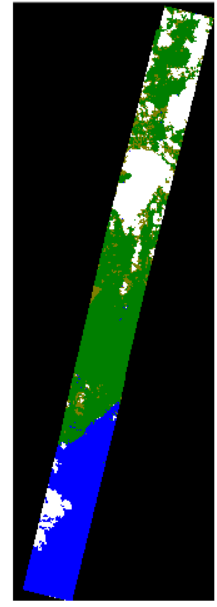
(a) EarthExplorer:  
10-19% cloud coverage



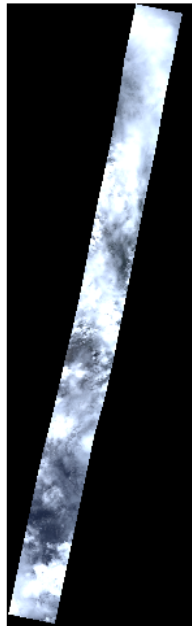
(b) This work:  
0.5% cloud coverage



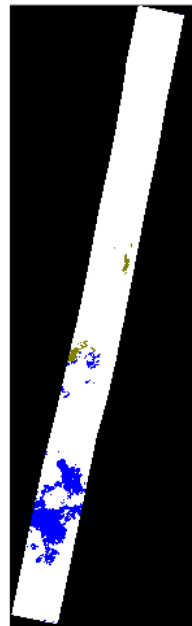
(c) EarthExplorer:  
40-49% cloud coverage



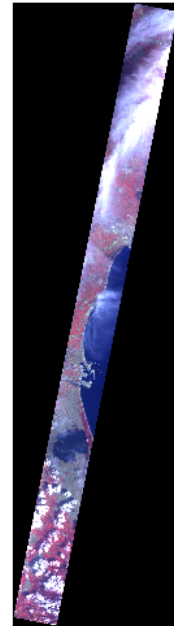
(d) This work:  
23% cloud coverage



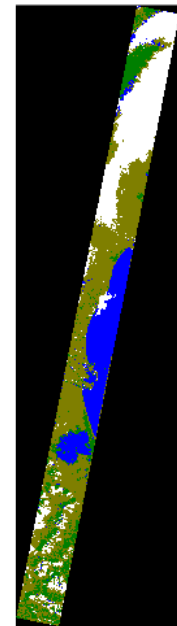
(e) EarthExplorer:  
90-99% cloud coverage



(f) This work:  
95% cloud coverage



(g) EarthExplorer:  
10-19% cloud coverage



(h) This work:  
28% cloud coverage

Fig. 4: A visual comparison of RGB images (left) for several Hyperion test data scenes against the results from our Supervised Spectral Classifier (right) with a training set of 4 classes. For the classified images, white = clouds, green = vegetation, blue = water, brown = desert/ dry land. Subfigures a) to f) are scenes over the big island of Hawaii showing a range of cloud coverage amounts. Subfigures g) and h) show the coastal region of Valencia, Spain with a good mix of all four classes. The classifier results generally appear to be visually consistent with RGB images, though the calculations for classified cloud coverage are not in complete agreement with USGS. This may be because of a different treatment of very thin cloud "haze" in cloud coverage calculations.



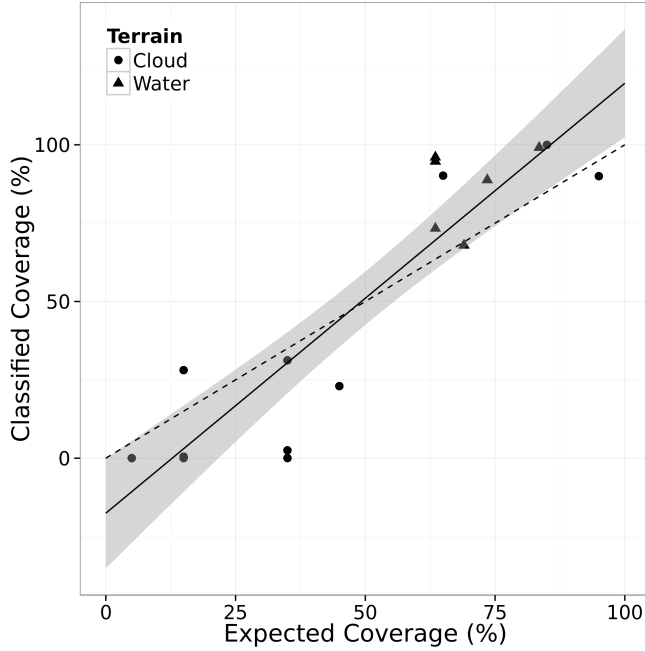


Fig. 5: Comparison of expected cloud and water coverages from USGS vs. coverages calculated from our classifier. Expected water points (triangles) are calculated from island scenes as described in the text. Expected cloud coverage estimates (circles) are taken from USGS EarthExplorer quoted cloud coverage for each image. The linear regression is the solid black line, and the grey shaded area is the 95% confidence interval. A 1-1 relationship is shown as a dashed black line for comparison.

for that image. The expected water coverage is calculated from scenes of islands that are completely contained within the image. We can then calculate expected water coverage by removing the known fractional land area of the islands and the USGS reported cloud coverage. We fit a regression line to the data, which shows an overall consistent relationship between the classified results and expected estimates.

#### F. Viewing analytic results

For convenience, each analytic produces a report after each run of the Wheel. These reports are built from the JSON results stored in Accumulo and are accessible to the public via a web page. The generated reports contain spectral and geospatial information about the scene analyzed as well as analytic results. An overview summary report is created for all daily data processed by an analytic in one run of the Wheel in addition to reports for individual scenes. These reports are generated and viewable immediately upon completion of the scan of new data available each day at the following address: <http://matsu-analytics.opensciencedatacloud.org/>. Analytic products are also made programmatically accessible through a Web Map Service.

#### IV. FUTURE WORK

The Matsu Wheel allows for additional analytics to be easily slotted in with no change to the existing framework so that we can continue to develop a variety of scanning analytics over these data. We are extending our existing Supervised Spectral Classifier to use specifically over floodplain regions to aid in flood detection for disaster relief. We are also planning to develop a similar analytic to aid in the detection of fires.

The analytics we described here are all detection algorithms, but we can also apply this framework and the results of our current analytics to implement algorithms for prediction. For example, our future work includes developing Wheel analytics for the prediction of floods. This could be done using the following approach:

- 1) Develop a dataset of features describing the observed topology of the Earth.
- 2) Use the topological data to identify "flood basins," or regions that may accumulate water around a local minimum.
- 3) Determine the relationship between detected water coverage in flood basins and the volume of water present.
- 4) Use observed water coverage on specific dates to relate the water volume in flood basins with time.
- 5) Use geospatial climate data to relate recent rainfall amounts with water volume, which then provides a simple model relating rainfall to expected water coverage at any pixel.

This proposed scanning analytic would provide important information particularly if implemented over satellite data with global and frequent coverage, such as data from the Global Precipitation Measurement (GPM) mission [16] [17]. Our future work involves continuing to develop the Matsu Wheel analytics and apply this framework to additional Earth satellite datasets.

#### V. SUMMARY

We have described here the Project Matsu Wheel, which is what we believe to be the first working application of a Hadoop-based framework for creating analysis products from a daily scan of available satellite imagery data. This system is unique in that it allows for new analytics to be dropped into a daily process that scans all available data and produces new data analysis products. With an analytic Wheel scanning framework, the data need to be read in only once, regardless of the number or types of analytics applied, which is particularly advantageous when large volumes of data, such as those produced by Earth satellite observations, need to be processed by an assortment of analytics.

We currently use the Matsu Wheel to process daily spectral data from NASA's EO-1 satellite and make the data and Wheel analytic products available to the public through the Open Science Data Cloud and via analytic reports on the web.

A driving goal of Project Matsu is to develop open source technology for satellite imagery analysis and data mining analytics to provide data products in support of human assisted disaster relief. The open nature of this project and

its implementation over commodity hardware encourages the development and growth of a community of contributors to develop new scanning analytics for these and other Earth satellite data.

#### ACKNOWLEDGMENT

Project Matsu is an Open Commons Consortium (OCC)-sponsored project supported by the Open Science Data Cloud. The source code and documentation is made available on GitHub at (<https://github.com/LabAdvComp/matsu-project>). This work was supported in part by grants from Gordon and Betty Moore Foundation and the National Science Foundation (Grant OISE- 1129076 and CISE 1127316).

The Earth Observing-1 satellite image is courtesy of the Earth Observing-1 project team at NASA Goddard Space Flight Center. The EarthExplorer cloud coverage calculations are available from the U.S. Geological Survey on [earthexplorer.usgs.gov](http://earthexplorer.usgs.gov).

#### REFERENCES

- [1] N. Backman, K. Pattabiraman, R. Fonseca, and U. Cetintemel, "C-mr: Continuously executing mapreduce workflows on multi-core processors," in *Proceedings of third international workshop on MapReduce and its Applications Date*. ACM, 2012, pp. 1–8.
- [2] J. Zeng and B. Plale, "Data pipeline in mapreduce," in *eScience (eScience), 2013 IEEE 9th International Conference on*. IEEE, 2013, pp. 164–171.
- [3] R. Kienzler, R. Bruggmann, A. Ranganathan, and N. Tatbul, "Stream as you go: The case for incremental data access and processing in the cloud," in *Data Engineering Workshops (ICDEW), 2012 IEEE 28th International Conference on*. IEEE, 2012, pp. 159–166.
- [4] K. R. Jackson, L. Ramakrishnan, K. Muriki, S. Canon, S. Cholia, J. Shalf, H. J. Wasserman, and N. J. Wright, "Performance analysis of high performance computing applications on the amazon web services cloud," in *CloudCom*, 2010, pp. 159–168.
- [5] D. Hearn, C. Digenis, D. Lencioni, J. Mendenhall, J. B. Evans, and R. D. Welsh, "Eo-1 advanced land imager overview and spatial performance," in *Geoscience and Remote Sensing Symposium, 2001. IGARSS '01. IEEE 2001 International*, vol. 2, 2001, pp. 897–900 vol.2.
- [6] J. Pearlman, S. Carman, C. Segal, P. Jarecke, P. Clancy, and W. Browne, "Overview of the hyperion imaging spectrometer for the nasa eo-1 mission," in *Geoscience and Remote Sensing Symposium, 2001. IGARSS '01. IEEE 2001 International*, vol. 7, 2001, pp. 3036–3038 vol.7.
- [7] R. L. Grossman, M. Greenway, A. P. Heath, R. Powell, R. D. Suarez, W. Wells, K. P. White, M. P. Atkinson, I. A. Klampanos, H. L. Alvarez, C. Harvey, and J. Mambretti, "The design of a community science cloud: The open science data cloud perspective," in *SC Companion*, 2012, pp. 1051–1057.
- [8] T. White, *Hadoop - The Definitive Guide: Storage and Analysis at Internet Scale (3. ed., revised and updated)*. O'Reilly, 2012.
- [9] J. Dean and S. Ghemawat, "Mapreduce: Simplified data processing on large clusters," in *OSDI*, 2004, pp. 137–150.
- [10] <https://accumulo.apache.org/>.
- [11] M. K. Griffin, S. M. Hsu, H.-H. Burke, S. M. Orloff, and C. A. Upham, "Examples of eo-1 hyperion data analysis," *Lincoln Laboratory Journal*, vol. 15, no. 2, pp. 271–298, 2005.
- [12] F. Ip, J. Dohm, V. Baker, T. Doggett, A. Davies, R. Castao, S. Chien, B. Cichy, R. Greeley, R. Sherwood, D. Tran, and G. Rabideau, "Flood detection and monitoring with the autonomous sciencecraft experiment onboard eo-1," *Remote Sensing of Environment*, vol. 101, no. 4, pp. 463 – 481, 2006. [Online]. Available: <http://www.sciencedirect.com/science/article/pii/S0034425706000228>
- [13] H. hua K. Burke, S. Hsu, M. K. Griffin, C. A. Upham, and K. Farrar, "Eo-1 hyperion data analysis applicable to cloud detection, coastal characterization and terrain classification," in *IGARSS*, 2004, pp. 1483–1486.
- [14] F. Pedregosa, G. Varoquaux, A. Gramfort, V. Michel, B. Thirion, O. Grisel, M. Blondel, P. Prettenhofer, R. Weiss, V. Dubourg, J. Vanderplas, A. Passos, D. Cournapeau, M. Brucher, M. Perrot, and E. Duchesnay, "Scikit-learn: Machine learning in Python," *Journal of Machine Learning Research*, vol. 12, pp. 2825–2830, 2011.
- [15] <http://earthexplorer.usgs.gov/>.
- [16] [http://www.nasa.gov/mission\\_pages/GPM/main/index.html](http://www.nasa.gov/mission_pages/GPM/main/index.html).
- [17] S. P. Neeck, R. K. Kakar, A. A. Azarbarzin, and A. Y. Hou, "Global Precipitation Measurement (GPM) L-6," in *Society of Photo-Optical Instrumentation Engineers (SPIE) Conference Series*, ser. Society of Photo-Optical Instrumentation Engineers (SPIE) Conference Series, vol. 8889, Oct. 2013.